International Journal of Thin Films Science and Technology

http://dx.doi.org/10.18576/ijtfst//130309

Optoelectronic characteristics for $(Cu_{1-x}\ A_{gx})_2\ ZnSnS_4$ films

A. Ahmed Elshafie, A. A. Showahy and E. R. Shaaban *

Physics Department, Faculty of Science, Al-Azhar University, Assiut 71542, Egypt

Received: 4 Feb. 2024, Revised: 16 Aug. 2024, Accepted: 22 Aug. 2024
Published online: 1 Sep. 2024

Abstract: Thick films of $(Cu_{1-x}\ A_{gx})_2\ ZnSnS_4$ (CAZTS), with a thickness of 500 nm, were deposited using electron beam gun technology. This study explores how varying silver (A_g) content influences the properties of CAZTS films. Structural characteristics were investigated using X-ray diffraction (XRD). Film thickness and refractive index were determined from transmission spectra using Swanpoel's method, and high-precision thickness measurements were further confirmed with spectral ellipsometry, employing three optical layer models. The absorption and extinction coefficients were calculated from transmittance and reflectance data in the strong absorption region, with bandgaps assessed accordingly. The bandgap decreased from 1.75 eV to 1.51 eV as Ag content increased, highlighting the probable of CAZTS films as absorber layers in solar cells. A Ni/n-CdS/p-CAZTS/Pt heterojunction was successfully fabricated, and its photovoltaic performance was estimated. By changing Ag content, the current-voltage characteristics of the heterojunctions were examined, suggesting that CAZTS thin films are promising candidates for solar cell absorber materials.

Keywords: $(Cu_{1-x}\ A_{gx})_2\ ZnSnS_4$ layers, Structural analysis, Spectrophotometric T and R, Optical properties, Heterojunctions, I-V curves.

1 Introduction

Recently, Cu2ZnSnS4 (CZTS), a quaternary material, has drawn a lot of interest as a capable absorber material for solar cell systems. It has a kesterite crystal structure and is composed of earth-abundant, non-toxic similar zinc (Zn), tin (Sn), copper (Cu), and sulfur (S). Due to these characteristics, CZTS is a viable substitute for existing thin-film PV materials that use pricy and poisonous metals similar cadmium (Cd) and indium (In). All things considered, CZTS is a capable for thin-film PV requests because it is made up of numerous, non-toxic elements and has the right optical and electrical properties for solar cell technology. CZTS-based solar cells could replace conventional silicon-based and thin-film PV technologies as a result of additional study and development [1,2,3,4,5].

Since the spin coating is quick and inexpensive, it is a common technique for depositing CZTS thin films. The procedure entails coating a substrate with a thin layer of a precursor solution before rapidly spinning the substrate to equally disperse the solution. The precursor is then heated to form a solid CZTS coating on the substrate [6,7,8]. Another popular method for depositing CZTS thin films is sputtering. High-energy ions are used to bombard a target material in this process, causing atoms to be expelled and deposited onto a substrate. The composition and qualities of the CZTS film can be controlled by sputtering with a variety of gases, such as argon [9,10,11]. In thermal evaporation, the precursor substance is heated in a vacuum chamber until it vaporizes, and then allowed to deposit onto a substrate where it condenses into a solid film. High-quality CZTS films with good crystallinity and purity can be produced using this technique [12,13]. Pulsed Laser Deposition (PLD) is a process that ablates a target material with a high-energy laser before depositing it onto a substrate. With perfect control over the deposition rate and composition, this technique may make CZTS films that are very uniform, dense, and of the highest quality [14,15]. In order to generate a CZTS film, a preliminary film of electron-beam-evaporated precursors is heated in the presence of sulfur gas after being deposited onto a substrate by electron beam evaporation. Using this technique, superior CAZTS films with good regularity and crystallinity may be created [16,17]. In spray pyrolysis, a precursor solution is sprayed onto a hot substrate, which causes it to break down and produce a CZTS film. Although this technique is rather straightforward and can make large-area CZTS films, it can be hard to regulate the film's thickness and homogeneity [18,19].

* Corresponding author e-mail: esam_ramadan2008@yahoo.com

The PCE for pure CZTS solar cells is currently recorded at 9.2%, whereas the PCE for pure CZTSe solar cells is reported at 11.6%. Mixed CZTS/CZTSe solar cells have a PCE that is marginally higher at 12.6%. These efficiencies, however higher than those of CIGS and CdTe solar cells, which have shown efficiencies of up to 21.7%, are still below those of those solar cells. Notwithstanding their lower efficiency, CZTS-based solar cells continue to spark a lot of research interest because of their inexpensive, non-toxic, and readily available constituent materials. Researchers are investigating a number of methods to increase the stability and efficiency of CZTS-based solar cells, including optimizing deposition techniques, engineering the band structure, and creating new device topologies [20,21,22,23].

Highly effective $(Cu_{1-x}\ A_{gx})_2\ ZnSn(S,Se)_4$ solar cells were studied by Xue Yu and colleagues for the use in flexible Mo foil [23]. Cu2ZnSn(S,Se)4 encoded as (CZTSSe) junction' efficiency is significantly increased by cation substitution. The band gap of (CAZTSSe) thin layers can be changed in this study by doping with Agx (where x is the content of Ag ranging from 0 to 5%. Additionally, it was discovered that Ag doping could clearly raise the CAZTSSe absorber's average grain size from 0.4 to 1.1 mm. Furthermore, the open-circuit voltage (Voc) steadily drops as a result. An increase in power conversion efficiency (PCE) from 4.34% to 6.24% was achieved. The study aimed to assess how varying Ag content affects the structural, optical, and electrical properties of ultra-thin $(Cu_{1-x}\ A_{gx})_2\ ZnSnS_4$ layers, with x ranging from 0 to 0.5%. Film thickness and refractive index were determined from transmission spectra using Swanpoel's method, and high-precision thickness calculations were further confirmed with spectral ellipsometry, employing three optical layer models.The energy gap of the CAZTS films was determined from the strong absorption regions of their transmission and reflection spectra. Additionally, a p-n junction of Ni/n-CdS/p-CAZTS/Pt heterojunction was successfully fabricated, and the dark and light current-voltage characteristics of these heterojunctions were analyzed for various CAZTS layers with different Ag contents.

2 Experimental techniques

2.1 Chemicals

Silver nitrate Ag(NO3) as a source for Ag, copper (II) nitrate Cu(NO3)2 for obtained Cu, zinc acetate Zn(CH3COO)2 for formating the Zn atoms, stannous chloride encoded as (SnCl2), citric acid incarnated (C6H8O7) form, deionized water, sulfide amine solution, and pure alcohol were the components used to synthesis the CAZTS thin layers. Without any additional purification, all of the used compounds and precursors were used.

2.2 Constructing CAZTS layers

The silver, copper, zinc and antimony precursors mentioned in the chemicals section were used to prepare an aqueous solution prepared for the synthesis of CAZTS thin samples by dissolving mixtures of the four precursors in equal proportions equivalent to one mole/ liter. In order to produce a translucent solution, after 10 minutes of mixing and good stirring of the aqueous solution in the preparation flask, metal ions from the aforementioned precursors were added to citric acid (C6H8O7) and deionized water. As a complexing agent, citric acid (C6H8O7) was used. At 150°C, 6 mL of Sulphide amine solution was added to the flask and allowed to react for roughly 30 minutes. Following that, the CAZTS nanoparticles were separated via a centrifuge. Powder nanoparticles were dried in a vacuum oven to generate the CAZTS powder, which is the final product used to prepare thin films by thermal evaporation. These glass substrates were likewise cleaned with ultrasonic and allowed to air dry after numerous 30-minute rinses in distilled water and pure alcohol. The electron beam gun (DV 502 A-type) coating device was set and calibrated at a deposition rate close to 20 angstrom/second and at high pressure in the vacuum chamber of 10-7 mbar, to obtain thin films at fixed substrate temperature equal 200 oC. The influence of film thickness was minimized by putting the same weight on the boat with the same thickness of thin films using the FTM6 thickness monitor. With astonishing accuracy, the film thickness was determined using a spectroscopic ellipsometry method.

2.3 Characterization and measurements

X-ray diffraction (XRD) patterns (Cu-Kα1 radiation ($\lambda = 1.54056$) with a Philips diffractometer (1710)) were used to determine the structural phase and parameters such as crystallite size and strain. Optical characteristics were investigated using spectroscopic ellipsometry (SE) with a VASE (J. A. Woollam Co., Inc.), where data were collected across a wavelength range of 300 to 1100 nm at an incidence angle of approximately 70°. The SE data were analyzed with the J. A. Woollam Complete Ease software. Optical transmission and reflection spectra of the thin films were measured using a

double-beam, computer-controlled spectrophotometer (UV-2101, Shimadzu) over a wavelength range from 300 to 2500 nm. A CdS thin layer was deposited directly onto the CAZTS layer (5 μm thick) with varying Ag content on pre-cleaned glass substrates to fabricate a p-n junction, specifically n-CdS/p-CAZTS heterojunctions. The heterojunctions, consisting of "ITO (100 nm)/n-CdS/p-CAZTS/Mo (100 nm)," were fabricated by layering materials through thermal evaporation (CdS) and electron beam gun deposition (CAZTS, Mo, and ITO). This layered structure is essential for optoelectronic devices such as solar cells, with each material and deposition method chosen to achieve optimal device performance. Illumination current-voltage (I-V) characteristics were measured using a Keithley 2400 device under standard conditions with AM1.5G illumination and a power density of 1800 mW/cm² produced by a 150W lamp.

3 Results and discussion

3.1 EDX and Structural studies

A summary of the EDAX results of $(Cu_{1-x}\ A_{gx})_2\ ZnSnS_4$ thin layers is recorded in Table 1. The X-ray diffraction (XRD) patterns of $(Cu_{1-x}\ A_{gx})_2\ ZnSnS_4$ thin film with varying Ag content are presented in Fig 1(a). The XRD results confirm the formation of crystalline CAZTS phases.

x	Cu(mV)	Ag(at/%)	Zn(at/%)	Sn(at/%)	S(at/%)
0	20.43	0	11.83	11.71	56.03
0.1	18.54	1.989	11.93	11.82	55.73
0.2	16.69	3.969	11.9	11.81	55.63
0.3	14.59	5.998	11.8	11.79	55.83
0.4	12.49	8.35	11.94	11.75	55.47
0.5	10.55	10.01	11.97	11.81	55.66

Table 1: Summary of the EDAX results of $(Cu_{1-x}Ag_x)_2\,ZnSnS_4$ thin films with various Ag contents $(0, 0.1, 0.2, 0.3, 0.4, 0.5)$

The CAZTS thin layers exhibit diffraction peaks at 28.53°, 47.32°, and 56.19°, corresponding to the diffraction planes of (112), (220), and (312), respectively. These planes are extracted from JCPDS card with no.26-0575. This provides strong evidence for the formation of CAZTS in a tetragonal phase. Furthermore, the CAZTS layers exhibit a sharper peak at (112) plane, indicating an improvement in crystal quality with an increase in Ag content. Fig. 1(b) illustrates the peak shift of (112) plane. A shift is observed in the diffraction angle towards smaller angles with increasing Ag content. The shift towards smaller diffraction angles in XRD (X-ray diffraction) curves with increasing Ag (silver) content can be attributed to a decrease in the interatomic distance between the atoms in the crystal lattice of the sample. The position of the diffraction peaks depends on the spacing between the atoms in the crystal lattice, which is determined by the atomic radii and the crystal structure. As the Ag atoms are substituted for other atoms in the crystal lattice, the interatomic distance between the atoms changes, leading to a shift in the position of the diffraction peaks. As Ag has a smaller atomic radius compared to the Cu element, the substitution of Ag atoms for Cu atoms results in a decrease in the interatomic distance, and thus a shift towards smaller diffraction angles in the XRD curve. This behavior can be used to identify the presence of Ag in a sample and to study the impacts of Ag substitution on the crystal structure and properties of the material [24,25]. The Debye-Scherrer equation is commonly used to determine the average crystallite size in polycrystalline materials from X-ray diffraction data. The equations relate the crystallite size (D) and lattice strain (e) to the main X-ray wavelength (λ), the diffraction angle (Bragg's angle θ), and the full width at half maximum (β) of the diffraction peak [26,27]:

$$\mathrm{D} = \left(\frac{0.94}{\beta}\right) \cdot \frac{\lambda}{\cos\theta} \& \mathrm{e} = \frac{\beta}{4\tan\theta} \text{ and } \beta = \sqrt{\beta_{\mathrm{obs}}^2 - \beta_{\mathrm{std}}^2} \tag{1}$$

β is the widening equivalent of the difference in profile width between the films (β_{obs}) and the standard silicon (β_{std}). The size of the crystallites increased as a result of increasing the Ag content, as seen in Fig. 2, whereas the lattice strain values dropped with increasing Ag concentration. The size of crystallites rises when Ag content increases because it serves as a site of nucleation for the development of new crystals or as a catalyst for the production of existing crystals. This is due to the possibility of extra nucleation sites for crystal growth being provided by the existence of Ag atoms, which encourages the building of bigger crystals. Lattice strain, on the other hand, measures the departure from the ideal crystal structure and can be caused by a variety of things, such as impurities or flaws in the crystal lattice. Because more Ag atoms

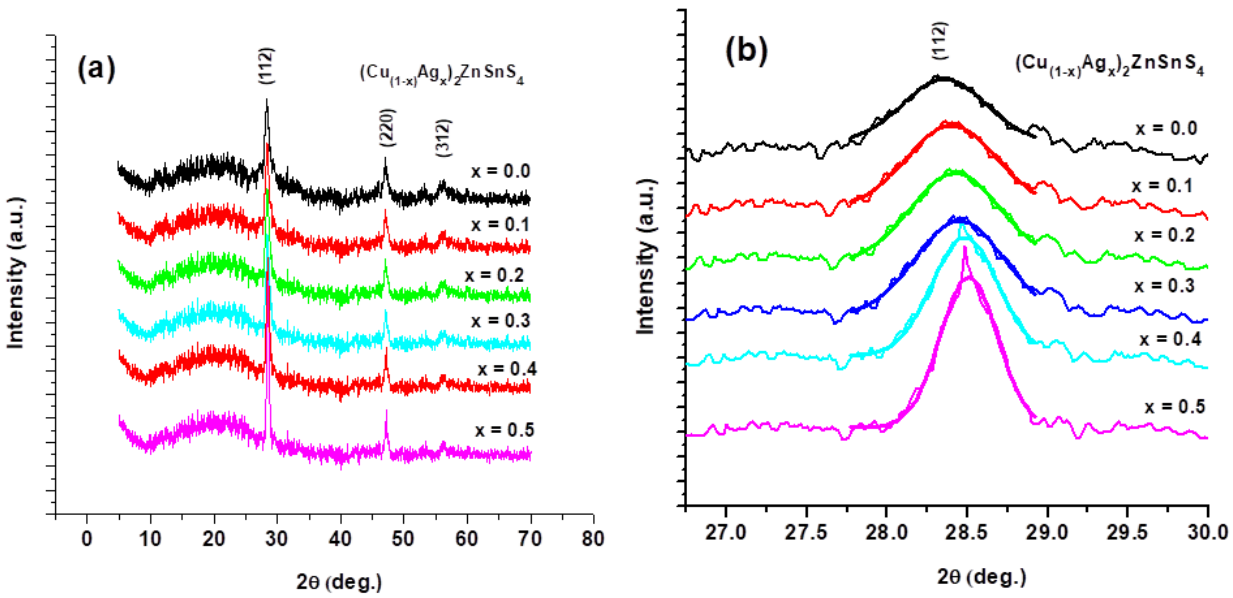

Fig. 1: (a) XRD patterns of $(Cu_{1-x}\ A_{gx})_2\ ZnSnS_4$ thin films, (b) peak shift of (112) plane.

can aid in reducing strain in the crystal lattice, the lattice strain values decrease as the Ag content rises. This is because Ag atoms have a higher atomic radius than the host metal atoms, which can cause the crystal lattice to be distorted. More Ag atoms are integrated into the lattice as the Ag concentration rises, which can aid in restoring the optimum crystal structure and lowering lattice strain. Overall, as a result of Ag's influences on crystal development and lattice distortion, an increase in Ag concentration causes crystallites to grow larger and lattice strain values to drop.

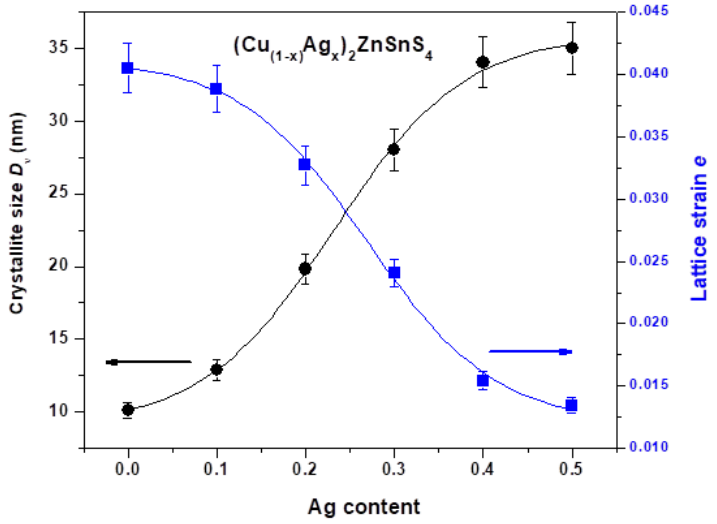

Fig. 2: crystallite size and lattice strain of $(Cu_{1-x}\ A_{gx})_2\ ZnSnS_4$ films as a function of Ag content.

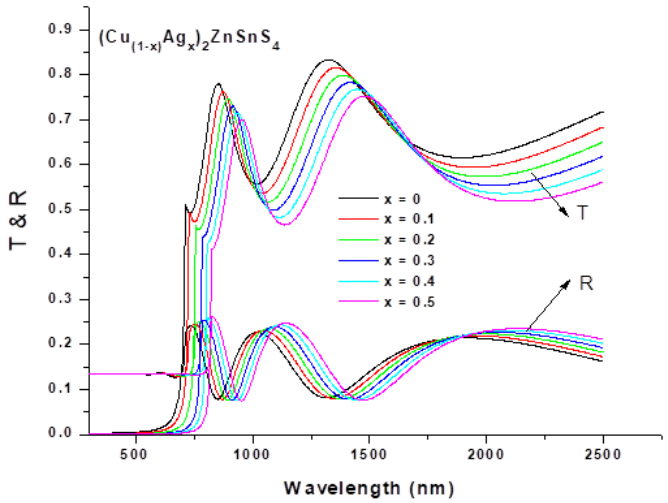

Fig. 3: The spectral variation of the transmittance and reflectance of $(Cu_{1-x}\ A_{gx})_2\ ZnSnS_4$ films with various Ag contents.

3.2 Optical properties

Fig. 4 describes the transmission and reflection spectra of thin films of $(Cu_{1-x}\ A_{gx})_2\ ZnSnS_4$ with varying Ag concentrations. These spectra were analyzed in the wavelength range of 300 to 2500 nm. It was observed that the transmittance (T) decreases with increasing Ag content in the film, particularly in the near-infrared region, where the lower transmission values were found to range from 60% to 70%. This decrease in transparency due to Ag doping makes these films suitable for use in the absorber layer of photovoltaic solar cells. The uniformity of film thickness, as well as the smoothness of the film surface, was confirmed by the presence of interference fringes. These fringes result from the coherence of multiple transmitted light waves at the interface between the film and substrate. This indicates that the film has a thickness uniformity of 0.5 μm and a smooth surface, which are desirable properties for various applications, including solar cells.

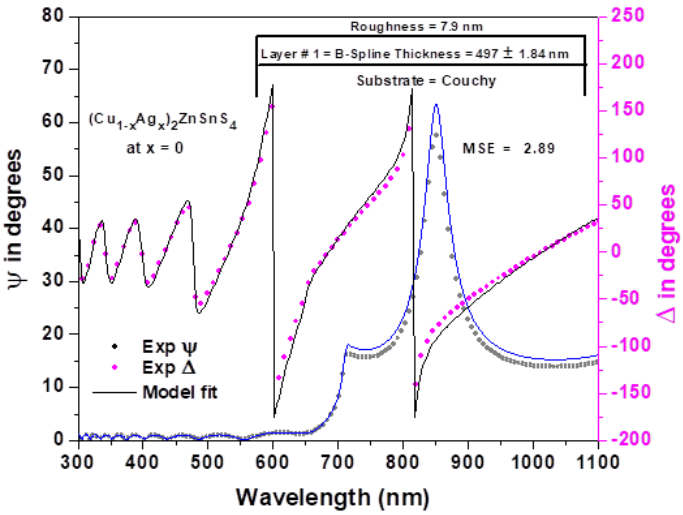

Fig. 4: Experimental and modeled ellipsometric optical parameters Psi and Delta for calculating the film thickness of $(Cu_{1-x}\ A_{gx})_2\ ZnSnS_4$ films.

The film thickness was determined using spectroscopic ellipsometry, where the parameters Ψ and Δ were measured over the wavelength range of 300 to 1100 nm. This measurement was carried out with a rotating compensator instrument, specifically the J.A. Woollam M-2000.

The methodological details are extensively covered in references [28,29,30,31]. The data acquisition is performed at a 70° incident angle. Utilizing the WVASE32 program, as illustrated in Fig. 5, a sophisticated approach employing three optical layer models is employed to accurately ascertain the film thickness. These models encompass a Cauchy layer representing the substrate, a B-spline layer representing the $(Cu_{1-x}\ A_{gx})_2\ ZnSnS_4$ film, and a surface roughness layer. This methodology ensures high precision in determining the film thickness.

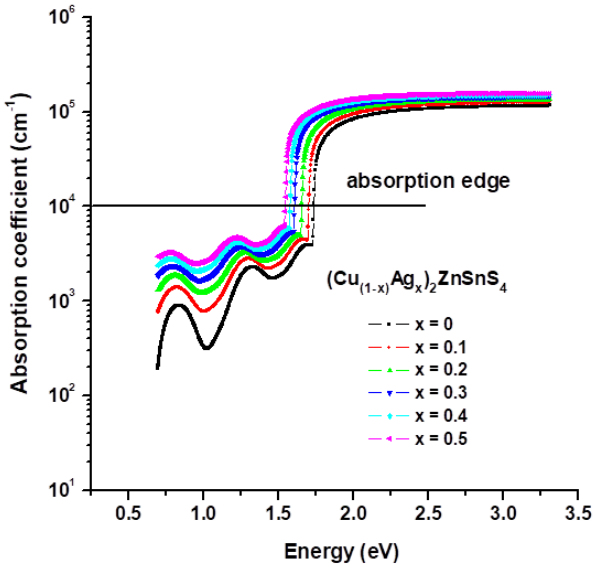

Fig. 5: The absorption coefficient versus photon energy of pure and Cu doped CdTe of (Cu1-xAgx)2ZnSnS4 films with various Ag contents.

The analysis of the figures suggests that as the Ag content increases, the transmittance in transparent regions also increases, while the reflectance decreases. This phenomenon can be attributed to several factors, including changes in the crystal structure or morphology of the thin films due to Ag substitution. The introduction of Ag into the $(Cu_{1-x}\ A_{gx})_2\ ZnSnS_4$ films may lead to a more organized crystal structure or a reduction in defects that would otherwise absorb or scatter light. This improvement in crystal structure or defect reduction enhances the transparency of the films. Additionally, higher Ag content may contribute to smoother film surfaces, thereby reducing scattering losses and facilitating better transmission of light through the material.Overall, the observed increase in transmittance and decrease in reflectance with increasing Ag content suggest that Ag doping positively influences the optical properties of the $(Cu_{1-x}\ A_{gx})_2\ ZnSnS_4$ films, potentially making them more suitable for various optoelectronic applications. However, the decrease in reflectance with increasing Ag content suggests alterations in the surface and electronic structure that make the surface less reflective. This could be due to a smoother surface, as mentioned, or changes in the electronic states at the surface, affecting how light interacts with the material. Increased Ag content might improve optical impedance matching between the film and its substrate, thus reducing the amount of light reflected from the surface. This effect would enhance the efficiency of optical devices by minimizing energy losses due to reflection. A decrease in reflectance, coupled with an increase in transmission in specific regions, might also suggest that absorption in other wavelength regions could be changing. This is critical for applications like photovoltaics, where controlling absorption profiles is essential for maximizing efficiency. The described changes in the optical properties of $(Cu_{1-x}\ A_{gx})_2\ ZnSnS_4$ thin films with different Ag concentrations have significant implications for photovoltaic applications, particularly in designing more efficient solar cells. By tailoring the Ag content, it might be possible to optimize these materials for maximum light absorption and conversion efficiency, leveraging the enhanced transmission and reduced reflectance. The transmission curve shows a sharp drop at the absorption edge, which is mainly due to the transition of electrons from the valence band (VBM) to the conduction band (CBM). Additionally, with increasing Ag concentration in $(Cu_{1-x}\ A_{gx})_2\ ZnSnS_4$, the absorption edge shifts towards longer wavelengths, indicating

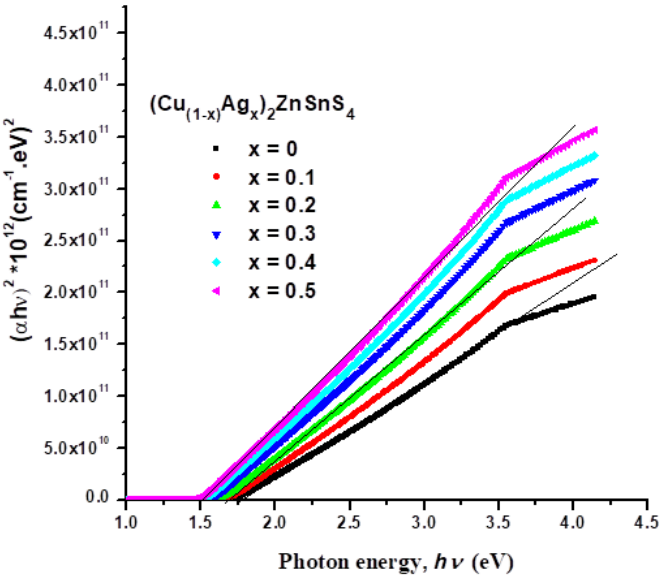

Fig. 6: $(\alpha h\nu)^2$ versus $h\nu$ of $(Cu_{1-x}\ A_{gx})_2\ ZnSnS_4$ films at different Ag contents.

a reduction in the fundamental energy gap of the material with higher Ag doping levels. Figure 6 displays the absorption coefficient as a function of photon energy for Ag-doped $(Cu_{1-x}\ A_{gx})_2\ ZnSnS_4$ films. This coefficient was calculated from transmission and reflection measurements in the strong absorption region, using the methodology detailed in references [32,33,34].

$$\alpha(\lambda) = \left(\frac{1}{\mathrm{d}}\right) \ln\left(\mathrm{X}' \times \mathrm{Y}'\right) \tag{2}$$

$$\mathrm{X}' = \left[\left(1-\mathrm{R}_1'\right)\left(1-\mathrm{R}_2'\right)\left(1-\mathrm{R}_3'\right)\right] / \left[2T\left(1-\mathrm{R}_2'\mathrm{R}_3'\right)\right] \tag{3}$$

and

$$\mathrm{Y}' = 1 + \left\{1 + \left[\mathrm{R}_1'\left(\mathrm{R}_2' + \mathrm{R}_3' - 2\mathrm{R}_2'\mathrm{R}_3'\right)\right] / \left(1-\mathrm{R}_2'\mathrm{R}_3'\right)\mathrm{A}^2\right]\right\}^{1/2} \tag{4}$$

In the provided relation for the absorption coefficient, d represents the film thickness, and the terms R_1', R_2', and denote the Fresnel reflection coefficients for the air-film interface, film-substrate interface, and substrate-air interface, respectively. The films exhibit a notably high absorption coefficient value, approximately $(\approx 105cm-1)$, indicating strong absorption properties. This high absorption coefficient renders the films suitable for application as an absorber layer in solar cells. Interestingly, the results indicate that the absorption coefficient decreases with increasing Ag concentration. Furthermore, it's observed that the absorption value undergoes a sudden decrease at the absorption edge, which also shifts towards lower energy levels as the level of Ag incorporation increases. This trend underscores the influence of Ag doping on the optical properties of the $(Cu_{1-x}\ A_{gx})_2\ ZnSnS_4$ films, offering insights into their potential application in optoelectronic devices.

The absorption coefficient $(\aleph)$, which is impacted by different of variables including the composition, thickness, and microstructure of the material, offers information on how strongly the material absorbs light at a specific wavelength in the instance of CAZTS/glass layers with varied Ag contents. One may ascertain the optical characteristics of these materials and their prospective uses in optoelectronics, photovoltaics, and other sectors by determining the absorption coefficient for varied Ag concentrations of CAZTS/glass layers [35,36,37,38].

CAZTS materials are quaternary semiconductors that have undergone substantial research in preparation for their prospective application in photovoltaic solar cells. Efficiency as a solar absorber is greatly influenced by the material's optical properties, particularly its energy band gap. For extracting the energy band gap of semiconductors, researchers frequently utilize the Tauc expression. It is based on a material's ability to absorb photons of a particular energy, as determined by the material's absorption coefficient. The following can be used to express the Tauc expression [39,40,41]:

$$(\alpha h\nu) = A'\left(h\nu - E_g^{opt}\right)^r \tag{5}$$

In this formula, r and A' incarnate exponent and constant. The index value, r is a parameter that depends on the nature of the band gap (direct or indirect) and determines the transition type from VB to CB. For the polycrystalline character of the CAZTS layers under investigation, the permitted direct transition is dominant with $(r = 1/2)$ [42,43,44]. Fig. 7 shows the plotting of $(\alpha h\nu)^2$ versus $h\nu$ for different Ag contents of CAZTS layer. The energy band gap E_g^{opt} was determined by subtracting the measured data's intercept from the absorption coefficient's linear extrapolation to zero after the measured data had been fitted to the Tauc expression. As the Ag concentration in the CAZTS layers increases, the band gap value for the CAZTS/glass film drops (see Fig. 7) as sigmoidal behavior. This is due to the possibility that the addition of Ag will cause some Zn and/or Cu sites in the CAZTS lattice to partially substitute. The band gap of the material decreases as a result, the impact of doping Ag (silver) atoms into a CAZTS (Copper Zinc Tin Sulfide) lattice, specifically how it affects the band gap of the material. Silver (Ag) has a lower electronegativity compared to Zinc (Zn) or Copper (Cu). Electronegativity is a measure of an element's tendency to attract electrons towards itself in a chemical bond. Because Ag has a lower electronegativity, it's more willing to give up its electrons. When Ag atoms are doped into the CAZTS lattice, they contribute electrons to the lattice. This is due to the lower electronegativity of Ag. These extra electrons can affect the electronic structure of the material. The extra electrons from the Ag doping contribute to the conduction band of the material. The conduction band is the energy band in a material where electrons are free to move and conduct electricity. When there are more electrons in the conduction band, the band gap decreases. Lowering the band gap means it requires less energy to excite an electron from the valence band (where electrons are normally located) to the conduction band [45,46,47]. This can have implications for the material's optical and electronic properties. Several other factors besides doping can affect the decrease of band gap of a material. These include structural factors [48], defects in the lattice and stress in the material's surface [49,50,51].

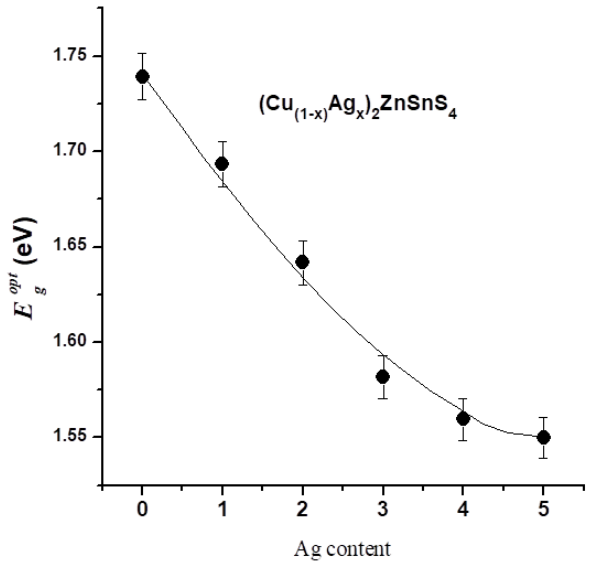

Fig. 7: Optical energy gap of $(Cu_{1-x}\ A_{gx})_2\ ZnSnS_4$ thin films as a function of Ag content.

The refractive index of semiconducting plays a vital role in the design and optimization of solar cells and photovoltaic devices. Several methods have been employed to calculate the refractive index of semiconductor thin films, as detailed in references [37,38,1,40,41,42]. In the case of Ag-doped $(Cu_{1-x}\ A_{gx})_2\ ZnSnS_4$ films [43,44]. The detailed procedure of this method is explained elsewhere [45,46]. Fig. 8(a, b) illustrates the envelope approach to the optical transmittance of $(Cu_{1-x}\ A_{gx})_2\ ZnSnS_4$ films at Ag concentrations of $x = 0$ and $x = 0.5$, serving as examples of the method's implementation. This methodology provides valuable insights into the optical properties of the films, facilitating their characterization and potential application in optoelectronic devices. Fig. 9 illustrates the spectral variation of the refractive index for Ag-doped $(Cu_{1-x}\ A_{gx})_2\ ZnSnS_4$ films. The figure exhibits a normal dispersion behavior, wherein the refractive index increases with decreasing wavelength. An important observation is that as the

level of Ag incorporation increases, there is an overall increase in the refractive index of the films. This rise in refractive index correlates with the observed decrease in the optical band gap energy with increasing Ag incorporation level. This correlation is well-established through various empirical models [47,48,49]. The Lorentz-Lorenz equation directly links the refractive index with the polarizability of the material. The substitution of Cu, which has a lower atomic radius (1.17 Å), with Ag, having a larger atomic radius (1.45 Å), leads to an increase in the density of the material. Consequently, this substitution enhances the polarizability of the material [50], thereby contributing to the observed increase in the refractive index with increasing Ag content. However, another contributing factor could be the reduction in crystallinity and grain size of $(Cu_{1-x}\ A_{gx})_2\ ZnSnS_4$ films as the Ag concentration increases. This decrease in crystallinity and grain size may also contribute to the observed increase in refractive index [51].

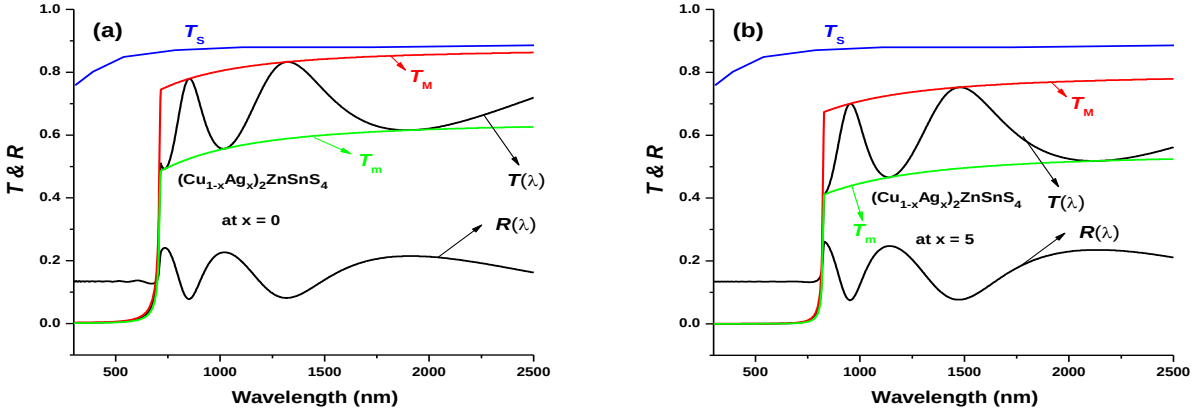

Fig. 8: (a, b): The optical transmittance, $T(\lambda)$ and reflectance $R(\lambda)$ spectra of $(Cu_{1-x}\ A_{gx})_2\ ZnSnS_4$ (with $x = 0$ and 5at.%) thin films at thickness 0.5 μm.

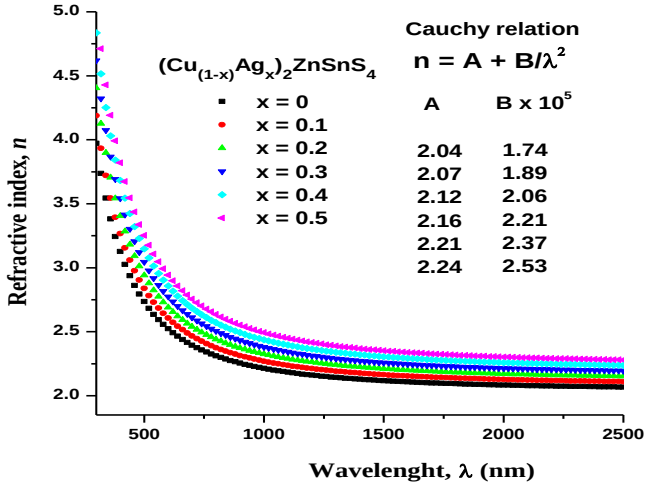

Fig. 9: The spectral dependence of the refractive of $(Cu_{1-x}\ A_{gx})_2\ ZnSnS_4$ films with different Ag concentrations.

The extinction coefficient (k) of $(Cu_{1-x}\ A_{gx})_2\ ZnSnS_4$ films is determined using a specific equation $\alpha = 4\pi k/\lambda$. The spectral performance of the extinction coefficient for these films is depicted in Fig. 10. Notably, the extinction coefficient experiences a significant drop to its lowest value in the strong absorption region, attributed to the absorption of incident photons at the central absorption edge. Furthermore, the figure illustrates that the overall extinction coefficient increases

with higher levels of Ag incorporation. This trend further supports the effect of Ag doping on the optical behaviors of the films, underscoring its potential significance in various optoelectronic applications.

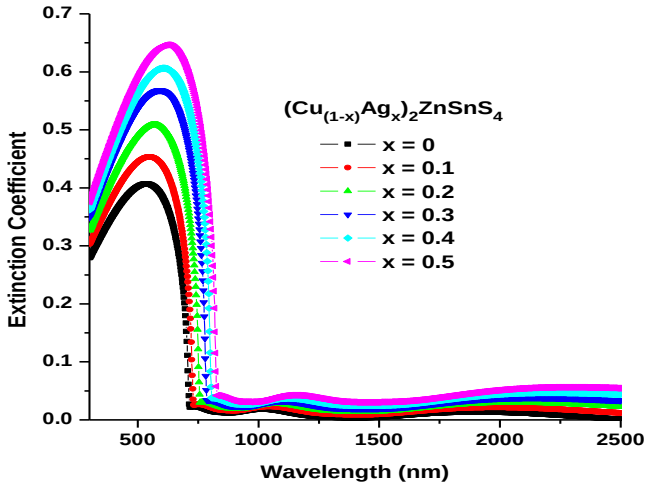

Fig. 10: The spectral variation of k for $(Cu_{1-x}\ A_{gx})_2\ ZnSnS_4$ films with different Ag concentrations.

3.3 Photovoltaic characteristics for p-n junction

The p-n junctions were manufactured with thin CdS layer (∼80 nm) as n-type and 0.5 µm of $(Cu_{1-x}\ A_{gx})_2\ ZnSnS_4$ layer with variable Ag content (n- CdS/p-$(Cu_{1-x}\ A_{gx})_2\ ZnSnS_4$) as depicted in Fig. 11. It should be noted that the main parameters of the fabricated p-n junctions are extracted as a function of Ag content of p-$(Cu_{1-x}\ A_{gx})_2\ ZnSnS_4$) layer to determine the behaviour of dark (I-V) characteristics for the forward and reverse bias applied in the range of (-2 to 2 volts).

The relationship between current (I) and applied voltage (V) in a diode can be described by the diode equation, which is given by [52]:

$$I = I_0 \left(e^{\frac{qV}{nkT}} - 1 \right) \tag{6}$$

Where I is the diode current, Io is the reverse saturation current (a characteristic parameter of the diode), is the electronic charge which equals to $(1.6 \times 10^{-19} C)$, V is the applied voltage across the diode, n is the ideality factor, typically between 1 and 2, k is Boltzmann's constant, T is the temperature in Kelvin. This equation describes the behavior of ideal diodes under different biasing conditions. In practice, diode characteristics can be affected by various factors such as temperature, doping concentration, and material properties. So, the specific parameters of the fabricated diode will determine its behavior. The quality factor of the fabricated diode is a measure of how "good" the diode is at storing and releasing energy efficiently. The quality factor can vary significantly depending on factors like the purity of the materials used, the manufacturing process, and the intended operating conditions.

Fig. 12 (a) depicts the dark (I-V) characteristics for the fabricated junction in forward and reverse bias for the variable Ag content with applied voltage in the specified ranges. The increasing current with increasing voltage indicates that the solar cell is operating in the forward bias region. In the forward bias region, the diode allows current to flow more easily as the voltage increases. This is typical behavior for a solar cell when it's generating power under illumination. In general, the higher current in forward bias than reverse bias because in the forward bias region, the p-n junction generates electrical current as it absorbs photons and converts their energy into electron-hole pairs, allowing them to flow through the external circuit. In the reverse bias region, the flow of current is significantly reduced as the diode junction becomes more resistant to current flow. It is clearly seen that the current increases as the Ag content increase in $(Cu_{1-x}\ A_{gx})_2$ $ZnSnS_4$ layer. Fig. 12 (b) depicts the dependence of the I on the applied V in the forward and reverse biases. Solar cell efficiencies are often reported under this standard spectrum because it closely approximates sunlight conditions on

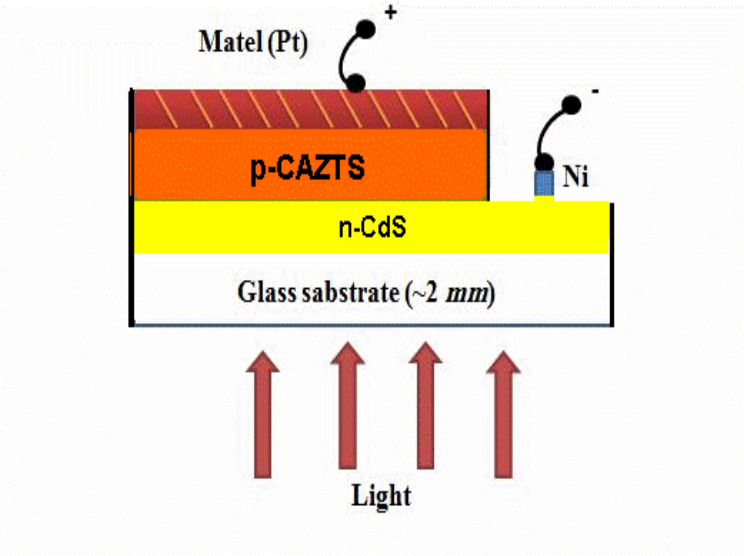

Fig. 11: The diagram of fabricated p-n junction n-CdS/p-CAZTS.

Earth's surface. The observed increase in current with increasing Ag content in the $(Cu_{1-x}\ A_{gx})_2\ ZnSnS_4$ layer indicates that the incorporation of silver (Ag) into the layer is enhancing the performance of the solar cell. Here's a three possible explanation for this behavior: the first is the addition of Ag to the $(Cu_{1-x}\ A_{gx})_2\ ZnSnS_4$ layer may modify its electronic band structure. This modification can lead to a reduction in the bandgap energy of the material as mentioned in optical section. A narrower bandgap allows the absorption of photons with lower energy, extending the absorption spectrum of the solar cell into the visible and near-infrared regions. As a result, more photons can be absorbed, leading to an increase in the generation of electron-hole pairs and hence an increase in current. The second is, the increasing of Ag content may also improve the charge carrier transport properties within the $(Cu_{1-x}\ A_{gx})_2\ ZnSnS_4$ layer. This could include enhancing carrier mobility or reducing recombination losses. Improved charge carrier transport facilitates more efficient extraction of generated carriers, leading to higher current output. The third is the rising of Ag may influence the interfaces between the $(Cu_{1-x}\ A_{gx})_2\ ZnSnS_4$ layer and adjacent CdS layers within the p-n junction structure. Optimizing these interfaces can reduce losses due to recombination and enhance charge carrier collection efficiency, contributing to the observed increase in current.

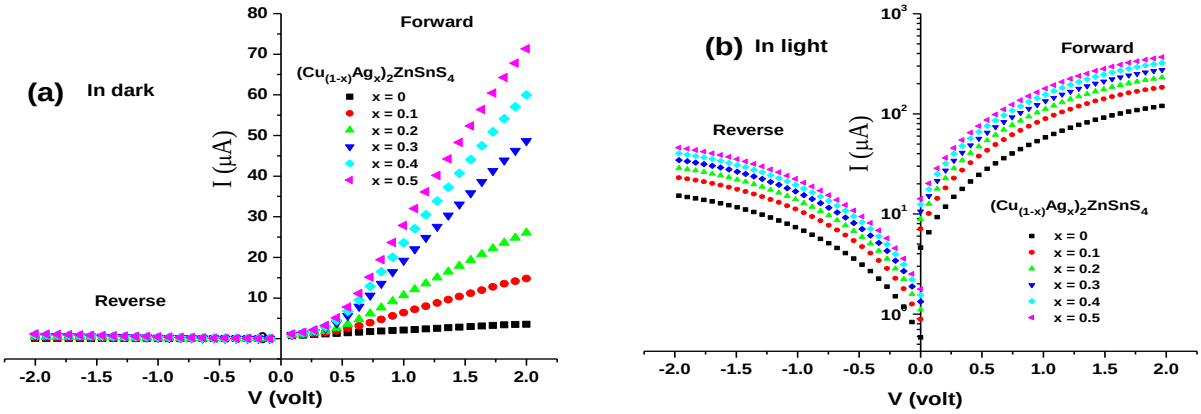

Fig. 12: (a)The dark (I-V) characteristics for the fabricated solar cell and(b) the I-V characteristics under standard solar simulated illumination (AM1.5G, 100mW/cm2) for the p-n junction solar cell in the range of (-2, 2) volts for $(Cu_{1-x}\ A_{gx})_2\ ZnSnS_4$ thin films.

4 Conclusions

Thin films with 0.5 μm of $(Cu_{1-x}\ A_{gx})_2\ ZnSnS_4$ (CAZTS) were deposited by the thermal evaporation technology. This work investigated the effects of varying the Ag content on the structural, and optical properties of thin layers of CAZTS, which were prepared via the thermal evaporation method. The XRD patterns revealed that the thin layers had a Kesterite band structure, with a crystallite size ranging from 10 to 34 nm. Using spectroscopic ellipsometry, the three optical layer models (adhesive layer of the substrate/B-spline layer of $(Cu_{1-x}\ A_{gx})_2\ ZnSnS_4$ films/surface roughness layer) were applied to estimate the film thickness with high precision which calibrated in terms of Swanepoel's method. Also, The refractive index of the films were determined by envelope method that suggested by Swanepoel. In a strong absorption region for transmittance and reflectance, the absorption coefficient thus the extinction coefficient, were calculated for $(Cu_{1-x}\ A_{gx})_2\ ZnSnS_4$ films. The optical properties of the CAZTS/glass film were found to improve with increasing Ag content, as demonstrated by an increase in the optical constants (n) and (k). Additionally, the direct transition energy decreased from 1.75 to 1.51 eV. The Ni/n-CdS/p-CAZTS/Pt heterojunction was well constructed, and the primary photovoltaic characteristics of the n-CdS/p-CAZTS junctions were examined for use in solar cells. The material's conduction band is improved by the additional electrons from the Ag doping. When a photovoltaic cell is worked in forward bias with illumination, it products power. Different Ag contents of the CAZTS layers were used to determine the (current-voltage) characteristics of the heterojunctions. All things considered, this work offers insightful information on the characteristics and behavior of CAZTS thin layers with different Ag contents, information that may help advance the formation of solar cell technologies that are more effective.

Conflicat of Interest

The authors declare that there is no conflict of interest regarding the publication of this paper.

References

[1] M. D. Oisamoje and E. E. Oisamoje, Exploring the economic and environmental benefits of solar energy generation in developing countries: the nigerian perspective, *Journal of Energy Technologies and Policy* **3**(6) (2013) 23–29.
[2] K. Obaideen, M. N. AlMallahi, A. H. Alami, M. Ramadan, M. A. Abdelkareem, N. Shehata and A. Olabi, On the contribution of solar energy to sustainable developments goals: Case study on mohammed bin rashid al maktoum solar park, *International Journal of Thermofluids* **12** (2021) p. 100123.
[3] S. Ren, H. Wang, Y. Li, H. Li, R. He, L. Wu, W. Li, J. Zhang, W. Wang and L. Feng, Rapid thermal annealing on znmgo window layer for improved performance of cdte solar cells, *Solar energy materials and solar cells* **187** (2018) 97–103.
[4] S. CHEN, X. GONG, A. WALSH and S.-H. WEI, Crystal and electronic band structure of cu2znsnx4 (x, *Applied physics letters* **94**(4) (2009).
[5] G. Agawane, A. Kamble, S. Vanalakar, S. Shin, M. Gang, J. H. Yun, J. Gwak, A. Moholkar and J. H. Kim, Fabrication of 3.01% power conversion efficient high-quality czts thin film solar cells by a green and simple sol–gel technique, *Materials letters* **158** (2015) 58–61.
[6] P. Fernandes, P. Salomé and A. Da Cunha, Cuxsnsx+ 1 (x= 2, 3) thin films grown by sulfurization of metallic precursors deposited by dc magnetron sputtering, *physica status solidi c* **7**(3-4) (2010) 901–904.
[7] P. Salomé, J. Malaquias, P. Fernandes, M. Ferreira, A. Da Cunha, J. Leitão, J. González and F. Matinaga, Growth and characterization of cu2znsn (s, se) 4 thin films for solar cells, *Solar Energy Materials and Solar Cells* **101** (2012) 147–153.
[8] S. K. Swami, A. Kumar and V. Dutta, Deposition of kesterite cu2znsns4 (czts) thin films by spin coating technique for solar cell application, *Energy Procedia* **33** (2013) 198–202.
[9] J.-S. Seol, S.-Y. Lee, J.-C. Lee, H.-D. Nam and K.-H. Kim, Electrical and optical properties of cu2znsns4 thin films prepared by rf magnetron sputtering process, *Solar energy materials and solar cells* **75**(1-2) (2003) 155–162.
[10] K. Jimbo, R. Kimura, T. Kamimura, S. Yamada, W. S. Maw, H. Araki, K. Oishi and H. Katagiri, Cu2znsns4-type thin film solar cells using abundant materials, *Thin solid films* **515**(15) (2007) 5997–5999.
[11] F. Liu, Y. Li, K. Zhang, B. Wang, C. Yan, Y. Lai, Z. Zhang, J. Li and Y. Liu, In situ growth of cu2znsns4 thin films by reactive magnetron co-sputtering, *Solar Energy Materials and Solar Cells* **94**(12) (2010) 2431–2434.
[12] A. Weber, H. Krauth, S. Perlt, B. Schubert, I. Kötschau, S. Schorr and H. Schock, Multi-stage evaporation of cu2znsns4 thin films, *Thin Solid Films* **517**(7) (2009) 2524–2526.
[13] O. Gunawan, T. K. Todorov and D. B. Mitzi, Loss mechanisms in hydrazine-processed cu2znsn (se, s) 4 solar cells, *Applied Physics Letters* **97**(23) (2010).
[14] K. Moriya, K. Tanaka and H. Uchiki, Cu2znsns4 thin films annealed in h2s atmosphere for solar cell absorber prepared by pulsed laser deposition, *Japanese Journal of Applied Physics* **47**(1S) (2008) p. 602.
[15] S. Pawar, A. Moholkar, I. Kim and S. Shin, Jh moon, ji rhee and jh kim: curr, *Appl. Phys* **10** (2010) 565–569.

[16] H. Katagiri, K. Saitoh, T. Washio, H. Shinohara, T. Kurumadani and S. Miyajima, Development of thin film solar cell based on cu2znsns4 thin films, *Solar Energy Materials and Solar Cells* **65**(1-4) (2001) 141–148.
[17] W. Daranfed, M. Aida, N. Attaf, J. Bougdira and H. Rinnert, Cu2znsns4 thin films deposition by ultrasonic spray pyrolysis, *Journal of alloys and compounds* **542** (2012) 22–27.
[18] M. Valdes, G. Santoro and M. Vázquez, Spray deposition of cu2znsns4 thin films, *Journal of Alloys and Compounds* **585** (2014) 776–782.
[19] N. Shinde, R. Deokate and C. Lokhande, Properties of spray deposited cu2znsns4 (czts) thin films, *Journal of Analytical and Applied Pyrolysis* **100** (2013) 12–16.
[20] K. Sun, C. Yan, F. Liu, J. Huang, F. Zhou, J. A. Stride, M. Green and X. Hao, Over 9% efficient kesterite cu2znsns4 solar cell fabricated by using zn1–xcdxs buffer layer, *Advanced Energy Materials* **6**(12) (2016) p. 1600046.
[21] Y. S. Lee, T. Gershon, O. Gunawan, T. K. Todorov, T. Gokmen, Y. Virgus and S. Guha, Cu2znsnse4 thin-film solar cells by thermal co-evaporation with 11.6% efficiency and improved minority carrier diffusion length, *Energy Mater* **5**(7) (2015) p. 1401372.
[22] W. Wang, M. T. Winkler, O. Gunawan, T. Gokmen, T. K. Todorov, Y. Zhu and D. B. Mitzi, Device characteristics of cztsse thin-film solar cells with 12.6% efficiency., *Advanced energy materials* **4**(7) (2014).
[23] X. Yu, S. Cheng, Q. Yan, J. Yu, W. Qiu, Z. Zhou, Q. Zheng and S. Wu, Efficient (cu 1- x ag x) 2 znsn (s, se) 4 solar cells on flexible mo foils, *RSC advances* **8**(49) (2018) 27686–27694.
[24] A. Weber, R. Mainz and H. Schock, On the sn loss from thin films of the material system cu–zn–sn–s in high vacuum, *Journal of Applied Physics* **107**(1) (2010).
[25] M. El-Hagary, M. Emam-Ismail, E. Shaaban, A. Al-Rashidi and S. Althoyaib, Composition, annealing and thickness dependence of structural and optical studies on zn1- xmnxs nanocrystalline semiconductor thin films, *Materials Chemistry and Physics* **132**(2-3) (2012) 581–590.
[26] M. El-Hagary, S. H. Moustafa, H. Hashem, E. R. Shaaban and M. Emam-Ismail, Influences of mn doping on the microstructural, semiconducting, and optoelectronic properties of hgo nanostructure films, *Journal of the American Ceramic Society* **102**(8) (2019) 4737–4747.
[27] M. Emam-Ismail, M. El-Hagary, E. Shaaban and S. Althoyaib, Structural and optical investigation of nanocrystalline zn1- xnixs diluted magnetic semiconductor thin films, *Journal of alloys and compounds* **529** (2012) 113–121.
[28] M. Mohamed, A. Abdelraheem, M. Abd-Elrahman, N. Hadia and E. Shaaban, Composition dependence of structural and linear and non-linear optical properties of cds 1- x mn x semiconducting thin films, *Applied Physics A* **125** (2019) 1–19.
[29] H. G. Tompkins and J. N. Hilfiker, *Spectroscopic ellipsometry: practical application to thin film characterization* (Momentum Press, 2015).
[30] H. Fujiwara, *Spectroscopic Ellipsometry: Principles and Applications* (John Wiley & Sons, 2007).
[31] G. Jellison Jr, Spectroscopic ellipsometry data analysis: measured versus calculated quantities, *Thin solid films* **313** (1998) 33–39.
[32] J. Woollam *et al.*, Completeease software manual, *Lincoln, USA: JA Woollam Co* (2014).
[33] E. Shaaban, M. Soraya, M. Shapaan, H. S. Hassan and M. Samar, Applying wedge shape model for calculating both film thickness and optical constants of seszn films with high precision for optoelectronic devices, *Journal of Alloys and Compounds* **693** (2017) 1052–1060.
[34] L. Ding, T. Chen, Y. Liu, C. Y. Ng and S. Fung, Optical properties of silicon nanocrystals embedded in a sio 2 matrix, *Physical Review B—Condensed Matter and Materials Physics* **72**(12) (2005) p. 125419.
[35] F. Behzadi, E. Saievar-Iranizad and E. Pakizeh, Optical study on single-layer photoluminescent graphene oxide nanosheets through a simple and green hydrothermal method, *Journal of Photochemistry and Photobiology A: Chemistry* **364** (2018) 595–601.
[36] E. Pakizeh and M. Moradi, Effect of particle size on the optical properties of lead zirconate titanate nanopowders, *Journal of the American Ceramic Society* **101**(12) (2018) 5335–5345.
[37] E. Shaaban, M. Abd El-Sadek, M. El-Hagary and I. Yahia, Spectroscopic ellipsometry investigations of the optical constants of nanocrystalline sns thin films, *Physica Scripta* **86**(1) (2012) p. 015702.
[38] A. Qasem, A. A. Hassan, F. Rajhi, H.-A. S. Abbas and E. Shaaban, Effective role of cadmium doping in controlling the linear and non-linear optical properties of non-crystalline cd–se–s thin films, *Journal of Materials Science: Materials in Electronics* **33**(4) (2022) 1953–1965.
[39] J. Tauc, R. Grigorovici and A. Vancu, Optical properties and electronic structure of amorphous germanium, *physica status solidi (b)* **15**(2) (1966) 627–637.
[40] M. El-Hagary, S. H. Moustafa, H. Hashem, E. R. Shaaban and M. Emam-Ismail, Influences of mn doping on the microstructural, semiconducting, and optoelectronic properties of hgo nanostructure films, *Journal of the American Ceramic Society* **102**(8) (2019) 4737–4747.
[41] M. Emam-Ismail, M. El-Hagary, E. Shaaban and S. Althoyaib, Structural and optical investigation of nanocrystalline zn1- xnixs diluted magnetic semiconductor thin films, *Journal of alloys and compounds* **529** (2012) 113–121.
[42] M. Emam-Ismail, A. A. Gharieb, S. Moustafa, M. Mahasen, E. Shaaban and M. El-Hagary, Enhancement of multifunctional optoelectronic and spintronic applications of nanostructured cr-doped sno2 thin films by conducting microstructural, optical, and magnetic measurements, *Journal of Physics and Chemistry of Solids* **157** (2021) p. 110195.
[43] R. Swanepoel, Determination of the thickness and optical constants of amorphous silicon, *Journal of Physics E: Scientific Instruments* **16**(12) (1983) p. 1214.
[44] J. Manifacier, J. Gasiot and J. Fillard, A simple method for the determination of the optical constants n, k and the thickness of a weakly absorbing thin film, *Journal of Physics E: Scientific Instruments* **9**(11) (1976) p. 1002.

[45] A. Qasem, B. Alshahrani, H. Yakout, H.-A. S. Abbas and E. Shaaban, Tuning structural, optical, electrical and photovoltaic characteristics of n-type cds 1- x sb x layers for optimizing the performance of n-(cds: Sb)/p-si solar cells, *Applied Physics A* **127** (2021) 1–13.
[46] H. Elsaeedy, A. Qasem, H. Yakout and M. Mahmoud, The pivotal role of tio2 layer thickness in optimizing the performance of tio2/p-si solar cell, *Journal of Alloys and Compounds* **867** (2021) p. 159150.
[47] A. Khare, A. W. Wills, L. M. Ammerman, D. J. Norris and E. S. Aydil, Size control and quantum confinement in cu 2 znsns 4 nanocrystals, *Chemical communications* **47**(42) (2011) 11721–11723.
[48] C. Li, Z. Song, D. Zhao, C. Xiao, B. Subedi, N. Shrestha, M. M. Junda, C. Wang, C.-S. Jiang, M. Al-Jassim *et al.*, Reducing saturation-current density to realize high-efficiency low-bandgap mixed tin–lead halide perovskite solar cells, *Advanced Energy Materials* **9**(3) (2019) p. 1803135.
[49] D. Gacio, J. M. Alonso, J. Garcia, M. S. Perdigao, E. S. Saraiva and F. E. Bisogno, Effects of the junction temperature on the dynamic resistance of white leds, *IEEE Transactions on Industry Applications* **49**(2) (2013) 750–760.
[50] A. Qasem, H. Alrafai, B. Alshahrani, N. M. Said, A. A. Hassan, H. Yakout and E. Shaaban, Adapting the structural, optical and thermoelectrical properties of thermally annealed silver selenide (agse) thin films for improving the photovoltaic characteristics of the fabricated n-agse/p-cdte solar cells, *Journal of Alloys and Compounds* **899** (2022) p. 163374.
[51] A. Qasem, M. Mahmoud, H. Elsaeedy, M. S. Mostafa and E. Shaaban, Effective role of temperature in improving the structural, optical and photovoltaic characteristics for n-zn0. 5cd0. 5te/p-cdte solar cells, *Optical Materials* **122** (2021) p. 111746.
[52] H. Elsaeedy, A. Qasem, H. Yakout and M. Mahmoud, The pivotal role of tio2 layer thickness in optimizing the performance of tio2/p-si solar cell, *Journal of Alloys and Compounds* **867** (2021) p. 159150.